



Research paper

Photoluminescent properties of three lanthanide compounds of formulae $\text{LnCl}_3(\text{diphenyl}((5\text{-phenyl-4H-1}\lambda^4\text{-pyrazol-3-yl)methyl)phosphine oxide})_2$, Ln = Sm, Eu and Tb: X-ray structural, emission and vibrational spectroscopies, DFT and thermogravimetric studies

John S. Maass^a, Randall K. Wilharm^a, Rudy L. Luck^{a,*}, Matthias Zeller^b

^a Department of Chemistry, Michigan Technological University, 1400 Townsend Drive, Houghton, MI 49931, USA

^b Department of Chemistry, Purdue University, 560 Oval Drive, West Lafayette, IN 47907-2084, USA

ARTICLE INFO

Article history:

Received 14 October 2017

Received in revised form 22 November 2017

Accepted 23 November 2017

Available online 26 November 2017

Keywords:

Lanthanide compounds

Photoluminescent

TGA

Crystal structures

Pyrazole

Phosphine oxide

ABSTRACT

The synthesis and properties of a new sensitizing bidentate ligand, diphenyl((5-phenyl-4H-1 λ^4 -pyrazol-3-yl)methyl)phosphine oxide, **2**, capable of demonstrating the emissive properties of lanthanide elements, is described. Two ligands are attached to LnCl_3 moieties, Ln = Sm, Eu and Tb, resulting in complexes of formulae $\text{LnCl}_3(\mathbf{2})_2$. These complexes were structurally characterized by single-crystal X-ray crystallography and have geometries that are pentagonal bipyramidal with the two bidentate ligands in a cisoid conformation on the equatorial plane and the three chloride ligands in a *mer*-configuration. The coordination bond distances decrease from Sm to Tb paralleling the decrease in lanthanide ionic radii. The photoluminescent properties of these complexes were examined and, one of them, $\text{TbCl}_3(\mathbf{2})_2$, was assessed a Φ_F of ca. 1.00. DFT calculations were conducted to understand the mechanism of proton transfer in ligand **2** for a hydrogen atom hopping between nitrogen atoms on the pyrazolyl moiety and, to assess aspects of the coordination sphere of the lanthanide complexes.

© 2017 Elsevier B.V. All rights reserved.

1. Introduction

We had reported on the utilization of tertiary phosphine oxide ligands in the preparation of catalysts capable of the oxidation of olefins with some of these employing hydrogen peroxide as the oxygen source [1–4]. We also demonstrated the utilization of phosphinate ligands in the synthesis of dimeric [5], trimeric [6–8] and tetrameric [9,10] metal clusters. Phosphine oxide ligands have also been bonded to lanthanide elements for the production of photoluminescent materials. In some of these examples, the phosphine oxide ligand completes the coordination sphere of the lanthanide element and does not absorb radiation; some other separate N-atom based ligand provides this function [11–14]. In others, organic ligands that can absorb light are bonded directly to the phosphine oxide ligand [15]. The absorbance of light leading to an excited state, 1S , then intersystem crossing (ISC) leading to a triplet excited state, 3T , followed by energy transfer into one of several excited states of the lanthanide ion followed by the emission of light has been previously described [15]. Difficulties in

the syntheses of phosphorus containing ligands pertaining mainly to the air-sensitive nature of the P-atom, may be behind the few studies on visible/emitting phosphine ligands on transition metal complexes [16]. However, as lanthanides are hard Lewis acids [17], perhaps better stability is afforded from binding to an O-atom attached to the P-atom in the desired ligand, i.e., a phosphine oxide ligand.

Nitrogen atom, ring-based molecules such as pyridine [18], phenanthroline [19], phenylpyrazole [20], bipyridine [21], dipicolinates [22], and azaxanthone [23] have been reported to form complexes with lanthanides with interesting photoluminescent properties. Of these N-atom based ligands, pyrazoles bonded to palladium [24] and zinc [25] have also displayed luminescent properties. The importance of lanthanide complexes have been reviewed recently as they pertain to the fields of luminescent hybrid materials [26], biolabelling [27], nanoprobe with optical spectroscopy and bioapplications [28], and imaging and sensing [29].

We decided to synthesize a bidentate ligand that would take advantage of the coordinating capabilities of N- and O-donor atom ligands (by combining methyldiphenylphosphine oxide and phenylpyrazole) and the light capturing and transferring capabilities

* Corresponding author.

E-mail address: rluck@mtu.edu (R.L. Luck).

of the phenylpyrazole moiety. In this report, we outline the synthesis of this new ligand, 5-phenyl-4*H*-1 λ^4 -pyrazol-3-yl)methylphosphine oxide, illustrate how isomers of this ligand are produced based on the synthetic strategy, and analyze the interconversion of these isomers by theoretical and variable temperature NMR methods. The ligating ability of the ligand is also reported in the form of complexation of the ligand to three lanthanide elements (i.e., Sm, Eu and Tb) and the luminescent properties of these complexes are described.

2. Experimental

2.1. Materials

Chemicals were purchased from Sigma-Aldrich Chemicals and solvents were purified as needed. Elemental analyses were conducted by Galbraith Laboratories, Knoxville, TN. IR spectra were recorded on a PerkinElmer Spectrum One (neat) spectrometer. ^1H and ^{31}P NMR data were recorded on a Varian XL-400 spectrometer referenced to CDCl_3 or acetone d_6 and 85% H_3PO_4 respectively. The TGA analyses were conducted on a Shimadzu TGA-50 analyzer. Absorbance spectra were obtained using quartz cells in a Perkin Elmer Lambda 35 UV/Vis Spectrometer. Fluorescence spectra were obtained using quartz cells (solution) and glass capillaries (solid) on a Horiba (Jobin Yvon) Fluoromax-4 Spectrofluorometer. A comparative method, involving the use of well characterized samples with known Φ_{F} values was utilized to assess the Φ_{F} [30].

3. Synthesis of ligand

3.1. Preparation of $(\text{C}_6\text{H}_5)_2\text{PO}(\text{CH}_2\text{COCH}_3)$, **1**

Methyldiphenylphosphine oxide, 2.824 g. (0.013 mol), was dissolved in 90 ml dried THF and cooled to 0 °C with an ice bath under nitrogen. n -Butyl lithium in hexane, 1.5 M, 9.1 ml (0.014 mol) was added and the solution was cooled to -77 °C with an ethanol/liquid nitrogen bath. 1.5 ml (0.015 mol) of dried ethyl acetate was added dropwise and the solution allowed to warm to room temperature and then stirred for 3 h. The mixture was quenched with saturated ammonium chloride solution, the solvent evaporated and the crude product recrystallized from ethyl acetate. 0.780 g (0.003 mol) of $(\text{C}_6\text{H}_5)_2\text{PO}(\text{CH}_2\text{COCH}_3)$, **1**, was produced in a 23.2% yield. ^{31}P NMR (CH_2Cl_2): $\delta = 25.70$ ppm. ^1H NMR (400 MHz, CDCl_3): $\delta = 2.30$ (s, 3H, CH_3), $\delta = 3.58$ (d, $J_{\text{HP}} = 16$ Hz, 2H, CH_2), $\delta = 7.40$ –7.80 (m, 10H, $(\text{C}_6\text{H}_5)_2$). IR (cm^{-1}): 3316br, 3057w, 2947br, 1707vs ($\nu\text{C}=\text{O}$), 1438m, 1359m, 1223s, 1179vs ($\nu\text{P}=\text{O}$), 1120s, 1102sh, 733s, 692s.

3.2. Preparation of $(\text{C}_6\text{H}_5)_2\text{PO}(\text{C}_3\text{H}_2\text{N}_2\text{-C}_6\text{H}_5)$, **2**

Compound **1**, 1.292 g (0.005 mol) was dissolved in 50 ml of dried THF under nitrogen and cooled to 0 °C with an ice bath. In a separate flask, 10 ml of 1.5 M n -BuLi in hexane was added to 1.5 ml of diisopropylamine in 25 ml of dry THF under nitrogen and stirred for 20 min. The n -BuLi mixture was then added to the flask containing **1** slowly via a canula and allowed to stir for 30 min. The color of the solution changed from clear to dark red. The solution was cooled to -77 °C with an ethanol/liquid nitrogen bath and 0.625 ml of methyl benzoate added dropwise. The color of the solution turned yellow-red. This solution was allowed to warm to RT and left to stir for 1.75 h. The reaction mixture was then quenched with 5 ml of a saturated ammonium chloride solution. The solution was removed to give a yellowish oil which was then dissolved in 30 ml of ethanol. 1.28 g of (50%–60% in H_2O) hydrazine was added and the solution was allowed to stir overnight. Ligand **2**

in the form of a white precipitate, 0.639 g, was obtained by filtration in a 37.5% yield. An ^1H NMR spectrum of pure sample at this stage suggested that two isomers with a H atom attached to either of the two N atoms in the pyrazole moiety were produced. ^1H NMR of the isomers (400 MHz, CD_3SOCD_3): $\delta = 3.85$ (d, $J_{\text{HP}} = 12$ Hz, CH_2), $\delta = 3.95$ (d, $J_{\text{HP}} = 12$ Hz, 2H, CH_2), $\delta = 6.10$ (s, 1H, CH_1), $\delta = 6.32$ (s, 1H, CH_1), $\delta = 7.20$ –7.90 (m, 15H, $(\text{C}_6\text{H}_5)_3$ Fig. S1). One isomer could be isolated as it is soluble in acetone. Anal. Calc. for $\text{C}_{22}\text{H}_{19}\text{N}_2\text{OP}$: C, 73.73; H, 5.34. Found: C, 73.82; H, 5.44%. ^{31}P NMR (CH_2Cl_2): $\delta = 30.25$ ppm; (CDCl_3): $\delta = 30.70$ ppm; (THF): $\delta = 28.65$ ppm. ^1H NMR of a pure sample (400 MHz, CDCl_3): $\delta = 3.74$ (d, $J_{\text{HP}} = 12$ Hz, 2H, CH_2), $\delta = 6.36$ (s, 1H, CH_1), $\delta = 7.20$ –7.90 (m, 15H, $(\text{C}_6\text{H}_5)_3$), Fig. S2. IR (cm^{-1}): 3184–2892 multiple small ridges, 1573sh, 1564m, 1463s, 1436s, 1234m, 1170vs ($\nu\text{P}=\text{O}$), 1118s, 1103s, 1069m, 1027m, 998m, 955s, 917m, 837s, 806m, 791m, 766s, 747m, 731m, 695s, 684vs.

3.3. Preparation of $\text{SmCl}_3[(\text{C}_6\text{H}_5)_2\text{PO}(\text{C}_3\text{H}_2\text{N}_2\text{-C}_6\text{H}_5)]_2$, **3**

0.025 g (0.069 mmol) of $\text{SmCl}_3 \cdot 6\text{H}_2\text{O}$ was dissolved in 2.5 ml of THF and added to 0.047 g (0.131 mmol) of **2** which was dissolved in 10 ml of boiling THF in a 50 ml Erlenmeyer flask exposed to the atmosphere. The solution went from cloudy to clear at which stage heating was turned off and the mixture allowed to stir overnight. A white precipitate formed which was obtained by filtration resulting in 0.037 g (0.033 mmol) of **3**, 48.3% yield. The crude product was dissolved in methylene chloride, precipitated by the addition of hexanes, obtained by filtration and dried. Anal. Calc. for $\text{C}_{44}\text{H}_{38}\text{N}_4\text{O}_2\text{P}_2\text{Cl}_3\text{Sm} \cdot 0.3\text{CH}_2\text{Cl}_2$: C, 53.26; H, 3.89. Found: C, 53.29; H, 3.89%. IR (cm^{-1}): 3220br, 3058br, 2957br, 1589m, 1565m, 1489s, 1470s, 1431vs, 1397m, 1301m, 1263m, 1154vs, 1121vs, 1092vs, 1068s, 1011vs, 959m, 907br, 849s, 753s, 719s, 686vs.

3.4. Preparation of $\text{EuCl}_3[(\text{C}_6\text{H}_5)_2\text{PO}(\text{C}_3\text{H}_2\text{N}_2\text{-C}_6\text{H}_5)]_2$, **4**

This complex was prepared in a similar manner to that for complex **3** from 0.049 g (0.137 mmol) of **2** with 0.025 g (0.068 mmol) of $\text{EuCl}_3 \cdot 6\text{H}_2\text{O}$ and resulted in 0.057 g (0.051 mmol) of **4**, 74.6% yield. The crude produce was dissolved in methylene chloride, precipitated by the addition of hexanes, obtained by filtration and dried. Anal. Calc. for $\text{C}_{44}\text{H}_{38}\text{N}_4\text{O}_2\text{P}_2\text{Cl}_3\text{Eu} \cdot 0.3\text{CH}_2\text{Cl}_2$: C, 53.18; H, 3.90. Found: C, 53.34; H, 3.90%. IR (cm^{-1}): 3224br, 3055m, 2951m, 2869m, 1585sh, 1563s, 1497s, 1459s, 1431vs, 1387m, 1299m, 1271m, 1145vs, 1123vs, 1112vs, 1090vs, 1062m, 1013vs, 959m, 905br, 838s, 748m, 715s, 688vs.

3.5. Preparation of $\text{TbCl}_3[(\text{C}_6\text{H}_5)_2\text{PO}(\text{C}_3\text{H}_2\text{N}_2\text{-C}_6\text{H}_5)]_2$, **5**

This complex was prepared in a similar manner to that for complex **3** from 0.048 g (0.134 mmol) of **2** with 0.025 g (0.067 mmol) of $\text{TbCl}_3 \cdot 6\text{H}_2\text{O}$ and resulted in 0.041 g (0.036 mmol) of **4**, 54.36% yield. The crude produce was dissolved in methylene chloride precipitated by the addition of hexanes, obtained by filtration and dried. Anal. Calc. for $\text{C}_{44}\text{H}_{38}\text{N}_4\text{O}_2\text{P}_2\text{Cl}_3\text{Tb} \cdot 0.3\text{CH}_2\text{Cl}_2$: C, 52.81; H, 3.86. Found: C, 52.66; H, 4.00%. IR (cm^{-1}): 3230br, 3054br, 2963br, 2901bmp, 2867br, 1591s, 1562s, 1490vs, 1461s, 1434vs, 1388br, 1316sh, 1297m, 1268m, 1149vs, 1120vs, 1091s, 1076s, 1014vs, 962m, 915m, 843s, 795sh, 751s, 727s, 689vs.

3.6. X-ray crystallography

X-ray quality crystals for compound **3** were obtained by diffusion of hexanes into a THF solution of **3** and those for **4** and **5** were obtained by the slow diffusion of hexanes into methylene chloride solutions of compounds **3**–**5**. Diffraction data for all compounds were collected using a Bruker AXS SMART APEX CCD diffractometer

using monochromatic Mo K α radiation with the omega scan technique. Single crystals of compounds containing **3**, **4** and **5** were mounted on Mitegen micromesh supports using viscous oil flash-cooled to 100 K. Data were collected, unit cells determined, and the data integrated and corrected for absorption and other systematic errors using the Apex2 suite of programs [31]. The structures were solved by direct methods and refined by full matrix least squares against F² with all reflections using SHELXL [32]. In each structure, solvent molecules were present with varying degrees of disorder which were all satisfactorily accounted for. H atoms were refined mixed with the ones attached to the pyrazole moiety discovered in difference maps and refined freely and the rest at calculated positions. Final figures of merit for the three structures are listed in Table 1.

3.7. DFT calculations

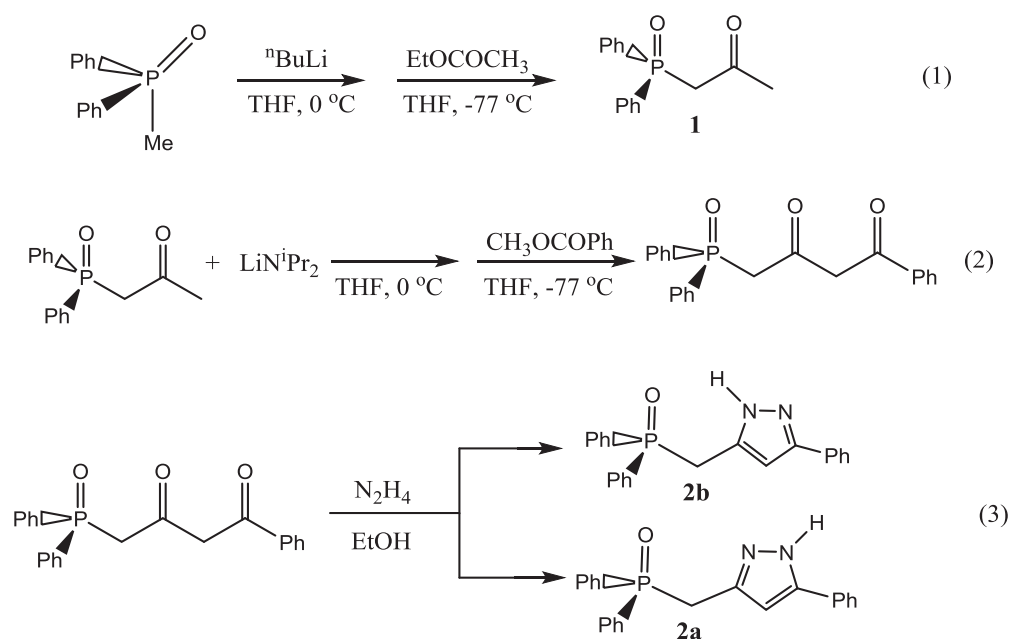
Superior, a high-performance computing infrastructure at Michigan Technological University, was used for the theoretical calculations presented in this publication. All calculations were carried out using Gaussian 09 [33]. Geometry optimizations were

3–5 was performed with atom positions derived from the crystal structure of **5**. The program GaussSum [39] was utilized in checking the progression of the various refinements.

4. Discussion

4.1. Ligand synthesis

The syntheses of the ligands **1** and **2** are outlined in Eqs. (1)–(3) and extreme care in the preparation of solvents and reactants is required in order to obtain reasonable yields of the compounds. Ligand **1** contained absorptions frequencies at 1707 and 1179 cm⁻¹ which were assigned to C=O and P=O stretches based on a theoretical calculation of the FTIR spectrum, Fig. S3 [33]. The NMR spectra for **1** were also unambiguous as signals for the methyl (s, δ 2.30), the methylene (d, δ 3.58) and the ¹H NMR and one signal at δ 25.70 for the P atom in the ³¹P NMR attest. Evidence for the formation of the two isomers of **2** (Eq. (3)) is in the ¹H NMR spectra of the crude product where two doublets at δ 3.85 and 3.95 were observed for the methyl group and two singlets for the pyrazole C–H atom at δ 6.10 and 6.32, Fig. S1.



performed using the B3LYP [34,35] functional with a 6-311+G(d,p) basis set for the ligand **2**, and the B3LYP [34,35] functional with D95V**++ and LanL2DZ (La) basis sets for the non-lanthanide and La elements, respectively, for calculations of generalized lanthanide complexes. This method was reported recently in a calculation with La substituting for Tb [36]. Alternatively, complexes **3–5** were handled computationally using the PBE/PBE functional with 6-31G* basis sets for the non-lanthanide elements and the Stuttgart RSC 1997 ECP basis set for each individual lanthanide element, i.e., Sm, Eu and Tb. The basis sets were downloaded from the Basis Set Exchange [37]. The computations for the isomerization of ligand **2** were conducted in vacuum and also including appropriate solvent fields with the PCM equilibrium solvation. Frequency calculations were performed at the B3LYP level of theory. Geometry optimization for the ligand **2** was performed with atom positions drawn initially and then optimized using Avogadro [38]. The geometry optimization for complexes

While a single pyrazole results from the reaction between hydrazine and a symmetrical β -dicarbonyl, with other reactants (i.e., unsymmetrical β -dicarbonyl) two isomeric pyrazoles are often isolated from the reaction mixture [40,41]. Interestingly calculations of ground state energy levels indicate that **2b**, with the H atom on the pyrazole ligand involved in an H-bond to the O atom attached to the P atom, is slightly more stable than **2a** by 4.24 and 1.98 kcal/mol based on calculations of ground state and THF solvation energies respectively at 298.15 K, see Table 2. It is possible to isolate one isomer as one, presumably **2b**, is more soluble in non-polar solvents than **2a** which may contain intermolecular H-bonds. Only one set of peaks are observed if acetone or dichloromethane is used to dissolve the mixture, see experimental details and Fig. S2. As the ground state energy levels indicate that **2b** was more stable than **2a**, it was of interest to see if a conversion of **2b** to **2a** could be accomplished that would allow for **2a** to coordinate in a bidentate manner to transition metals. Variable temperature NMR spectra

(25–130 °C) of **2** dissolved in DMSO d_6 (which contained adventitious H_2O) show that coalescence between the two isomers, i.e., **2a** and **2b**, is attained at a temperature of approximately 70 °C for the methylene H atoms and 85 °C for the methine H atoms, see Fig. 1. These temperatures allow for an estimation of the

activation energy barrier (ΔG^\ddagger) of 14.9 kcal/mol for the methylene peaks and 14.4 kcal/mol for the methine H atom [42,43]. This method of calculation is only an estimation as there are difficulties in accurately determining coalescence temperature and peak separation [42,43].

Table 1
Crystal Data and Refinement Details of complexes **3–5**.

| Compound reference | 3 :2.5THF | 4 :2CH ₂ Cl ₂ | 5 :1.5CH ₂ Cl ₂ |
|--|--|---|---|
| Chemical formula | (C ₄₄ H ₃₈ Cl ₃ N ₄ O ₂ P ₂ Sm)·2.5(C ₄ H ₈ O) | C ₄₄ H ₃₈ Cl ₃ EuN ₄ O ₂ P ₂ ·2(CH ₂ Cl ₂) | (C ₄₄ H ₃₈ Cl ₃ N ₄ O ₂ P ₂ Tb)·1.5(CH ₂ Cl ₂) |
| Formula Mass | 1153.695 | 1144.90 | 1109.395 |
| Crystal system | Monoclinic | Monoclinic | Triclinic |
| a/Å | 36.331(2) | 25.667(1) | 12.5225(7) |
| b/Å | 15.4655(7) | 15.497(1) | 13.3637(8) |
| c/Å | 25.7740(10) | 26.530(1) | 15.2391(9) |
| $\alpha/^\circ$ | 90 | 90 | 101.8140(9) |
| $\beta/^\circ$ | 131.3718(5) | 114.412(1) | 93.6495(9) |
| $\gamma/^\circ$ | 90 | 90 | 109.2976(9) |
| Unit cell volume/Å ³ | 10867.7(9) | 9609.2(8) | 2332.0(2) |
| Temperature/K | 100(2) | 100(2) | 100(2) |
| Space group | C2/c | P2 ₁ /n | P $\bar{1}$ |
| No. of formula units per unit cell, Z | 8 | 8 | 2 |
| Absorption coefficient, μ/mm^{-1} | 1.334 | 1.804 | 1.971 |
| No. of reflections measured | 35,578 | 119,246 | 34,332 |
| No. of independent reflections | 13,301 | 23,819 | 11,469 |
| R_{int} | 0.0296 | 0.0341 | 0.0256 |
| Final R indices ($I > 2\sigma(I)$) | $R_1 = 0.0369$, ^a $R_2 = 0.0998$ ^{b,c} | $R_1 = 0.0254$, ^a $R_2 = 0.0592$ ^{b,d} | $R_1 = 0.0221$, ^a $R_2 = 0.0548$ ^{b,e} |
| R indices (all data) | $R_1 = 0.0462$, ^a $R_2 = 0.1077$ ^{b,c} | $R_1 = 0.032$, ^a $R_2 = 0.0633$ ^{b,d} | $R_1 = 0.0237$, ^a $R_2 = 0.056$ ^{b,e} |
| Goodness of fit on F^2 | 0.986 | 1.05 | 1.013 |
| CCDC number | 1528931 | 1528932 | 1528933 |

$$^a R_1 = \sum ||F_o| - |F_c|| / \sum |F_o|.$$

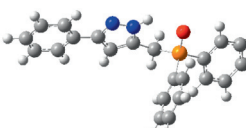
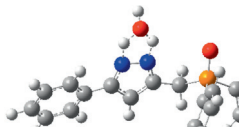
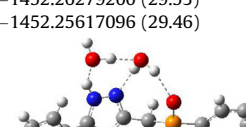
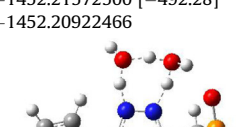
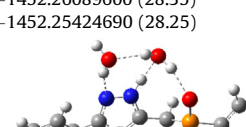
$$^b R_2 = [\sum [w(F_o^2 - F_c^2)]^2] / \sum [w(F_o^2)]^{1/2}.$$

$$^c w = 1 / [\sigma^2(F_o^2) + (0.0603P)^2 + 28.2500P] \text{ where } P = (F_o^2 + 2(F_c)^2) / 3.$$

$$^d w = 1 / [\sigma^2(F_o^2) + (0.0232P)^2 + 12.5065P].$$

$$^e w = 1 / [\sigma^2(F_o^2) + (0.0260P)^2 + 1.7927P].$$

Table 2
Internal energies in Hartrees for the various forms of ligand **2**. For **2a** and **2b** numbers within parentheses are the differences in kcal/mol between that molecule and the transition state. The numbers listed within square brackets for the transition state energies are for the one imaginary frequency in cm^{-1} obtained from the calculations.

| | 2a | Transition state | 2b |
|------------------------------|---|---|---|
| Ligand 2 |  |  |  |
| Gas Phase | −1375.79404300 (46.61) | −1375.71976800 [−1740.34] | −1375.80080500 (50.85) |
| SCRF-THF (298.15 °C) | −1375.81201400 (47.34) | −1375.73656700 [−1749.46] | −1375.81517400 (49.33) |
| SCRF-THF (339.15 °C) | −1375.80600695 (47.33) | −1375.73058546 | −1375.80918140 (49.32) |
| 2 + H ₂ O |  |  |  |
| Gas Phase | −1452.23807900 (24.51) | −1452.19902300 [−1640.42] | −1452.24238900 (27.21) |
| SCRF-THF (298.15 °C) | −1452.26279200 (29.53) | −1452.21572500 [−492.28] | −1452.26089600 (28.35) |
| SCRF-THF (339.15 °C) | −1452.25617096 (29.46) | −1452.20922466 | −1452.25424690 (28.25) |
| 2 + 2H ₂ O |  |  |  |
| Gas Phase | −1528.69454700 (13.63) | −1528.67282800 [−1292.16] | −1528.69526000 (14.08) |
| SCRF-THF (298.15 °C) | −1528.71037800 (13.17) | −1528.68939200 [−1024.47] | −1528.71031900 (13.13) |
| SCRF-THF (339.15 °C) | −1528.70313383 (13.01) | −1528.68240537 | −1528.70307417 (12.97) |

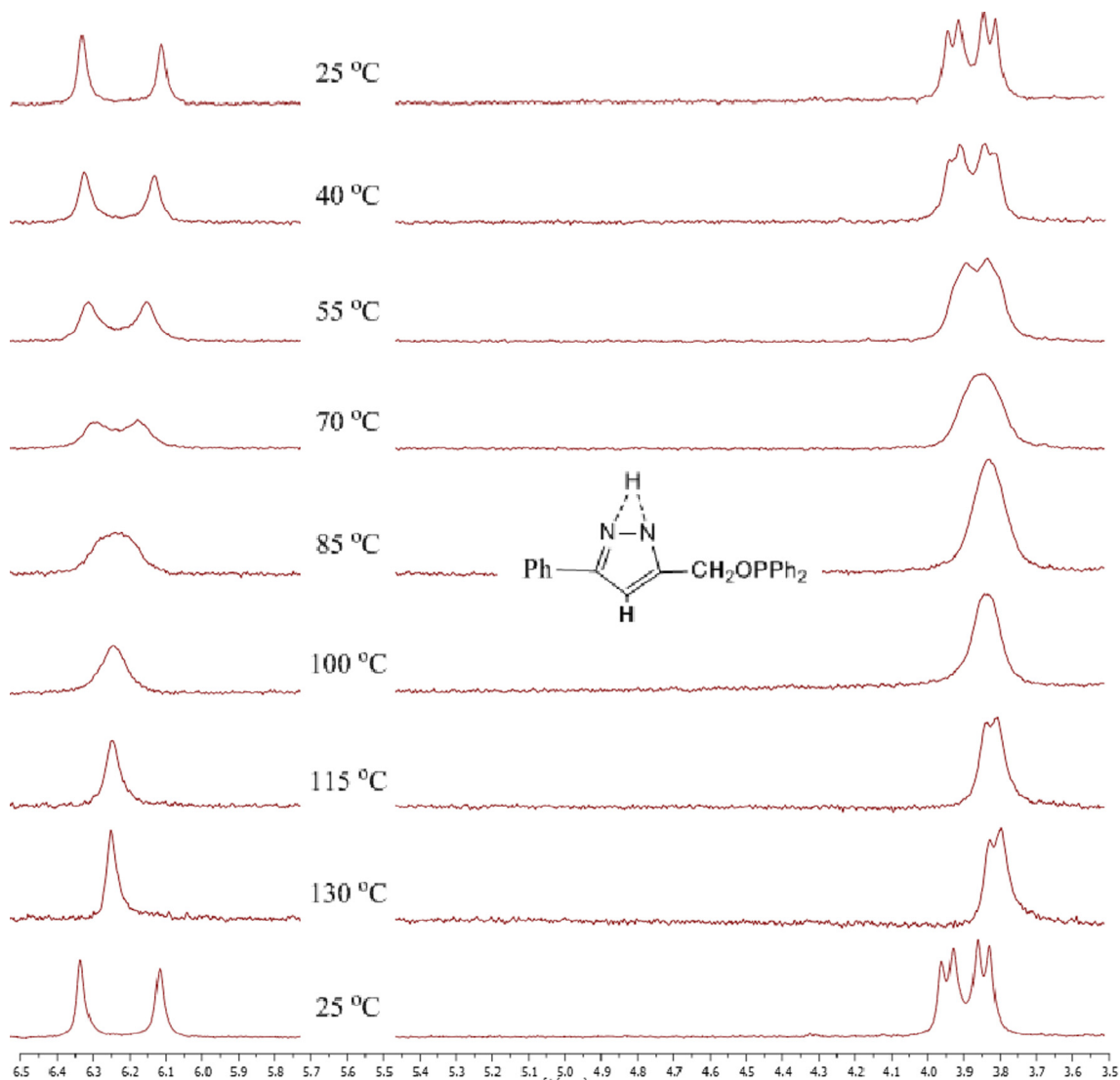
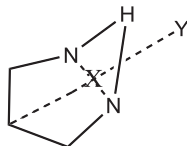


Fig. 1. ^1H NMR variable temperature of **2** (the “fleeting” transition state is depicted at 85 °C) in $\text{DMSO } d_6$ for the region where the pyrazole methine C-H (δ 6.10(s) and 6.32 (s)) and the CH_2 (δ 3.85(d) and 3.95(d)) resonate at 25 °C with the traces obtained in sequence from top to bottom.

Table 3
Geometry of the transition state of Ligand **2**.



| TS [‡] | $R_{\text{NN}}/\text{Å}$ | Distance $\text{H}\cdots\text{X}/\text{Å}$ | HXY° | NHN° |
|-----------------|--------------------------|--|--------------------|--------------------|
| Pyrazole [44] | 1.464 | 1.011 | 63.4 | 71.8 |
| 2 | 1.442 | 1.010 | 62.56 | 71.04 |

It has been previously demonstrated that while [1,5] hydrogen atom shifts are symmetry allowed for thermal reactions, the barriers for pyrazole, tetrazole and hydroxypyrazole are very high and on the order of 50 kcal/mol [44]. Similar values were obtained for the calculated transition barrier between **2a** and **2b** as shown in Table 2 for the ligand **2** with differences in energy levels of 50.85 and 46.61 between **2a** and **2b** respectively and the transition state.

This transition state, Table 3, contained the transient H atom at bond distances and angles consistent with that reported in the literature for pyrazole [44]. Interestingly, the transfer of the H atom is facilitated by the presence of water molecules judging from the decrease in the transition state energies in the gas phase for **2a(2b)** from 46.61(50.85) to 24.51(27.21) for one water molecule and 13.63(14.08) kcal/mol for two water molecules, see Table 2. The calculated values for the two water molecules are close to those estimated (14.4–14.9 kcal/mol) from the variable temperature NMR experiments. This would suggest that this is the pathway utilized. All of the transition states listed in Table 2 contained one negative frequency corresponding to motions of the H atom(s) in motion. Calculations in THF at 298.15 and 339.15 K, the boiling point of THF (the temperature where reactions were preformed), were also conducted and contained values not very different from those obtained in the gas phase. These calculations were important to demonstrate that even if mixtures of the ligand were obtained, subsequent chemistry that would utilize **2** in a bidentate manner is possible due to the H atom transfer should the more stable **2b** be produced. Surprisingly, there was a great difference in the transition state frequency for **2** with one water molecule, i.e., -1640.42 and -492.28 cm^{-1} , whereas the data for the other two, namely **2**

with two water molecules, were not that different, see Table 2. Lower transition state frequencies are indicative of plateau regions for the transition state due to a more stepwise nature in the transformation [45]. The conclusion from these calculations in Table 2 is that it is not necessary to isolate **2a** in order to synthesize complexes as the isomerization of **2b** to **2a** is facile in the presence of water molecules.

4.2. Synthesis and structures of the lanthanide complexes **3–5**

Reacting two equivalents of ligand **2** with one equivalent of $\text{LnCl}_3 \cdot 6\text{H}_2\text{O}$ in boiling THF resulted in the formation of complexes $\text{Ln}(\mathbf{2})_2\text{Cl}_3$, Ln = Sm **3**, Eu **4** and Tb **5**. These complexes were soluble in CH_2Cl_2 and CH_3CN but not stable for prolonged periods. On the basis of comparing the IR spectra of **2** to that of **3–5**, the

absorptions at 1154 , 1145 and 1149 cm^{-1} for **3–5** respectively can be assigned to the $\text{P}=\text{O}$ stretches in the compounds reflecting a slight decrease upon coordination. Attempts to obtain ^1H NMR spectra of these compounds were not successful due to the paramagnetic nature of the samples. Analyses of TGA spectra on bulk sample, Figs. S4–S6, revealed that each of samples **3–5** decomposed over the temperature range of $300\text{--}600\text{ }^\circ\text{C}$ in a step-wise manner with the Sm and Eu samples initially showing slight loss of solvent. The samples likely lost two of ligand **2** perhaps resulting in the formation of LnCl_3 , Ln = Sm, **3** (calcd. 73.6%, expt 65.5%), Eu, **4** (calcd. 73.5%, expt 69%) or Tb, **5** (calcd. 73.0%, expt. 66%), respectively. There have been reports of differences in weights (albeit much smaller) in TGA between calculated and experimental data on lanthanide-based samples [46] of much simpler composition

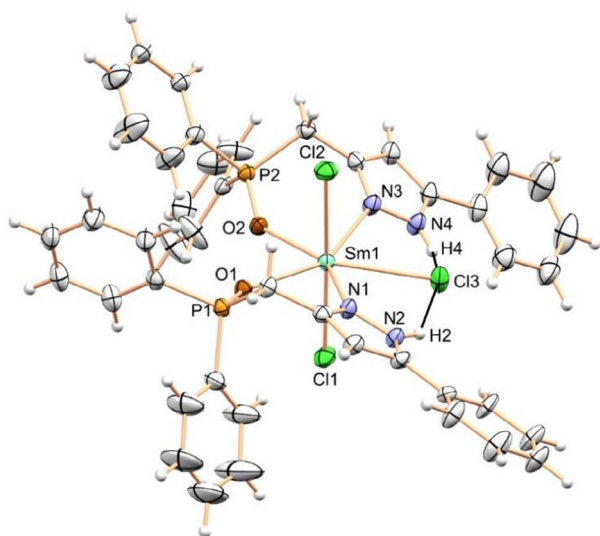


Fig. 2. Mercury [47] representation of the major form of **3**. Thermal ellipsoids are drawn at the 50% probability level and spheres of arbitrary radii represent hydrogen atoms. Solvent molecules are not drawn.

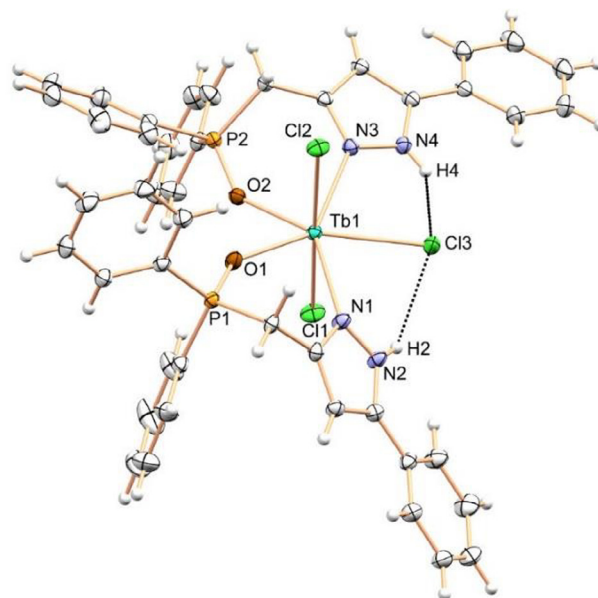


Fig. 4. Mercury [47] representation of **5**. Thermal ellipsoids are drawn at the 50% probability level and spheres of arbitrary radii represent hydrogen atoms. Solvent molecules are not drawn.

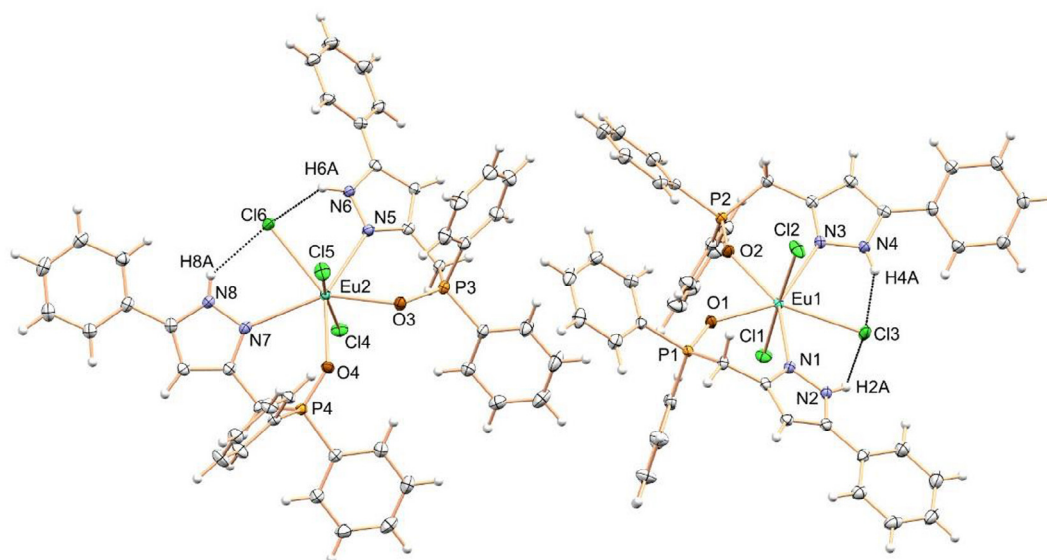


Fig. 3. Mercury [47] representation of the two molecules (**4'** on the right and **4'** on the left) constituting the asymmetric unit of **4**. Thermal ellipsoids are drawn at the 50% probability level and spheres of arbitrary radii represent hydrogen atoms. Solvent molecules are not drawn.

such as $\text{LaI}_3(\text{MeCN})_{1.25}$ suggesting that the decomposition may not be precise. If the final compounds were the oxyhalide or an oxide of formulae LnOCl and Ln_2O_3 , this would lead to lower residual mass remaining on the order of 18 and 21% respectively in contrast to the ~33% that was obtained on average for the three samples. Additionally if extra uncoordinated ligand was present, we would expect this to decompose and thus lower final weight percentages (i.e., perhaps <25%) would be obtained. Therefore, while the TGA results are not conclusive regarding purity of the samples (as the final composition is unknown), they do suggest that uncoordinated ligand **2** was not present in the samples.

X-ray suitable crystals of the complexes were obtained as described in the Experimental Section and crystal data and final structural parameters are listed in Table 1. Mercury [47] constructed thermal ellipsoid plots of the molecules are in Figs. 2–4 of **3–5** respectively and selected bond distances and angles are listed in Table 4. There is an asymmetry in the shape of these molecules to the extent that two phenyl groups on adjacent ligands attached to the P atom are roughly perpendicular to the pseudo plane produced by the equatorial (pentagonal coordination) and the data in Table 4 are presented such that these planes are in similar orientations. While the labels in Figs. 2 and 4, and, for **4'** in Fig. 3, are meaningful as indicated in Table 4, that for complex **4'** follows the same numbering scheme except that Cl(1) and Cl(2)

in **4'** relate to Cl(5) and Cl(4) in **4'** respectively. The asymmetric unit of complex **3** was refined to reveal 2.5 THF molecules some of which were disordered. One phenyl group attached to the pyrazole moiety on the ligand on the complex was also disordered. There were two molecules of **4** and four CH_2Cl_2 molecules comprising the asymmetric unit and of these one CH_2Cl_2 was disordered. Complex **5** contained two CH_2Cl_2 molecules in the asymmetric unit and one CH_2Cl_2 was situated around an inversion point. In all cases, disorder was accounted for with refinement [48].

All complexes have distorted pentagonal bipyramidal geometries. Two chloride ligands on apical positions with the remaining chloride and two ligand **2**'s (both bonded through the O atom and the N atoms on the pyrazole moiety proximal to the P=O bond) situated on the equatorial plane complete the coordination sphere to the central lanthanide element as evident in Figs. 2–4. Interestingly the O atoms on the ligands are cis to one another and this facilitates an H-bonded interaction between the H atoms on both pyrazole moieties distal to their respective P=O bonds and the equatorial chloride ligand. The data listed in Table 4 reveal that there are significant decreases in the coordination sphere bond lengths of these complexes going from **3** to **5** which is most likely related to the fact that the respective lanthanide element's radii decreases in the order Sm^{3+} (1.140 Å) > Eu^{3+} (1.120 Å) > Tb^{3+} (1.090 Å) as estimated in aqueous solutions [49].

Table 4

Selected bond distances and angles for **3–5** together with data from theoretical models. Data for La are based on the B3LYP functional and a LanL2DZ (La) basis set [35]. Data for Sm, Eu and Tb on the B3LYP PBEPBE functional with 6-31G* basis sets for the non-lanthanide elements and the Stuttgart RSC 1997 ECP basis set for each individual lanthanide [37].

| Complex | 3 | 4' | 4'' | 5 | La | Sm | Eu | Tb |
|---------------------------|------------|-------------|-------------|-------------|-----------|-----------|-----------|-----------|
| <i>Bond distances (Å)</i> | | | | | | | | |
| Ln(1)–O(1) | 2.3515(19) | 2.2882(15) | 2.3315(15) | 2.2937(13) | 2.485 | 2.405 | 2.392 | 2.352 |
| Ln(1)–O(2) | 2.360(2) | 2.3293(15) | 2.3342(15) | 2.2862(13) | 2.487 | 2.384 | 2.442 | 2.320 |
| Ln(1)–N(1) | 2.592(3) | 2.6685(18) | 2.6707(19) | 2.5788(15) | 2.809 | 2.697 | 2.718 | 2.609 |
| Ln(1)–N(3) | 2.615(3) | 2.6969(19) | 2.6383(19) | 2.5726(15) | 2.809 | 2.692 | 2.639 | 2.666 |
| Ln(1)–Cl(1) | 2.6450(8) | 2.6393(5) | 2.6495(6) | 2.6262(5) | 2.869 | 2.684 | 2.707 | 2.607 |
| Ln(1)–Cl(2) | 2.6997(8) | 2.6306(6) | 2.7018(5) | 2.6725(5) | 2.775 | 2.738 | 2.756 | 2.672 |
| Ln(1)–Cl(3) | 2.8182(7) | 2.7778(5) | 2.7654(5) | 2.7372(5) | 2.918 | 2.863 | 2.849 | 2.783 |
| O(1)–P(1) | 1.507(2) | 1.5060(16) | 1.5037(16)) | 1.5028(14) | 1.542 | 1.535 | 1.535 | 1.535 |
| O(2)–P(2) | 1.505(2) | 1.4998(16) | 1.5063(16) | 1.5020(13) | 1.538 | 1.534 | 1.533 | 1.534 |
| N(1)–N(2) | 1.357(3) | 1.360(2) | 1.358(2) | 1.354(2) | 1.352 | 1.349 | 1.347 | 1.349 |
| N(3)–N(4) | 1.356(3) | 1.362(2) | 1.363(2) | 1.355(2) | 1.352 | 1.348 | 1.347 | 1.348 |
| N(2)–H(2) | 0.83(5) | 0.84(3) | 0.86(3) | 0.83(3) | 1.024 | 1.035 | 1.035 | 1.033 |
| N(4)–H(4) | 0.85(3) | 0.83(3) | 0.83(3) | 0.80(3) | 1.024 | 1.036 | 1.035 | 1.035 |
| Cl(3)–H(2) | 2.30(4) | 2.26(3) | 2.25(3) | 2.52(3) | 2.231 | 2.162 | 2.161 | 2.188 |
| Cl(3)–H(4) | 2.33(3) | 2.22(3) | 2.34(3) | 2.46(3) | 2.226 | 2.142 | 2.202 | 2.134 |
| <i>Bond Angles (°)</i> | | | | | | | | |
| O(1)–Ln(1)–O(2) | 76.01(7) | 72.29(5) | 78.33(5) | 74.17(5) | 81.5 | 78.5 | 78.9 | 75.2 |
| O(1)–Ln(1)–N(1) | 71.59(7) | 71.81(5) | 72.27(5) | 72.02(5) | 68.9 | 72.4 | 70.57 | 73.4 |
| O(2)–Ln(1)–N(1) | 147.14(7) | 142.77(5) | 146.54(5) | 139.49(5) | 149.8 | 150.2 | 141.3 | 148.6 |
| O(1)–Ln(1)–N(3) | 145.82(7) | 142.15(5) | 150.87(5) | 139.70(5) | 149.2 | 146.2 | 153.1 | 141.9 |
| O(2)–Ln(1)–N(3) | 69.92(8) | 69.88(5) | 72.93(5) | 72.11(5) | 69.3 | 72.3 | 74.3 | 71.8 |
| N(1)–Ln(1)–N(3) | 141.81(8) | 144.66(5) | 133.15(6) | 146.97(5) | 138.0 | 132.8 | 134.1 | 137.3 |
| O(1)–Ln(1)–Cl(1) | 86.06(5) | 89.26(4) | 83.10(4) | 98.03(4) | 81.5 | 81.8 | 86.3 | 83.8 |
| O(2)–Ln(1)–Cl(1) | 91.48(6) | 92.30(4) | 85.93(4) | 83.59(3) | 81.8 | 81.6 | 80.4 | 83.4 |
| N(1)–Ln(1)–Cl(1) | 91.65(6) | 96.82(4) | 105.68(4) | 79.73(4) | 87.6 | 99.7 | 119.7 | 92.9 |
| N(3)–Ln(1)–Cl(1) | 97.24(6) | 93.65(4) | 99.30(4) | 99.48(4) | 84.8 | 109.6 | 87.6 | 110.4 |
| O(1)–Ln(1)–Cl(2) | 89.83(5) | 94.04(4) | 88.50(4) | 83.98(4) | 83.5 | 81.8 | 91.7 | 80.9 |
| O(2)–Ln(1)–Cl(2) | 92.21(6) | 87.65(4) | 86.07(4) | 95.95(3) | 83.7 | 86.07(4) | 79.5 | 89.4 |
| N(1)–Ln(1)–Cl(2) | 82.47(6) | 85.29(4) | 77.65(4) | 101.99(4) | 98.4 | 83.9 | 78.3 | 86.0 |
| N(3)–Ln(1)–Cl(2) | 88.86(6) | 83.07(4) | 84.95(4) | 78.25(4) | 102.3 | 73.8 | 85.0 | 80.3 |
| Cl(1)–Ln(1)–Cl(2) | 173.67(3) | 176.519(18) | 169.415(18) | 177.709(15) | 160.5 | 161.2 | 159.7 | 164.4 |
| O(1)–Ln(1)–Cl(3) | 142.98(5) | 143.09(4) | 141.40(4) | 143.06(3) | 139.0 | 140.46 | 131.6 | 144.7 |
| O(2)–Ln(1)–Cl(3) | 139.55(5) | 144.12(4) | 135.54(4) | 142.33(3) | 138.5 | 137.0 | 145.5 | 137.1 |
| N(1)–Ln(1)–Cl(3) | 73.29(5) | 72.90(4) | 72.01(4) | 72.29(4) | 71.7 | 72.5 | 72.6 | 73.3 |
| N(3)–Ln(1)–Cl(3) | 70.96(6) | 74.67(4) | 73.13(4) | 74.76(4) | 71.6 | 73.1 | 73.9 | 73.0 |
| Cl(1)–Ln(1)–Cl(3) | 83.59(3) | 84.467(19) | 81.91(2) | 84.667(17) | 108.0 | 86.8 | 85.5 | 86.5 |
| Cl(2)–Ln(1)–Cl(3) | 96.89(3) | 93.53(2) | 108.640(19) | 94.385(16) | 91.5 | 111.7 | 110.4 | 108.0 |
| P(1)–O(1)–Ln(1) | 139.52(12) | 143.31(9) | 139.80(9) | 144.16(8) | 142.7 | 138.8 | 138.9 | 138.6 |
| P(2)–O(2)–Ln(1) | 138.28(13) | 141.90(9) | 139.96(9) | 140.06(8) | 141.2 | 138.8 | 136.3 | 140.9 |
| H(2)–Cl(3)–H(4) | 155(1) | 167(1) | 154(1) | 136.3(8) | 172.1 | 162.6 | 165.1 | 173.9 |
| Equatorial sum | 361.8 | 361.6 | 368.7 | 365.4 | 363.0 | 368.8 | 370.3 | 366.7 |

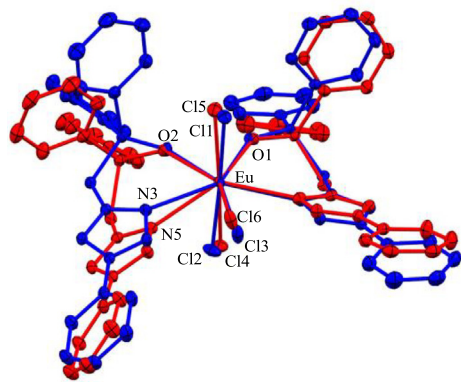


Fig. 5. Mercury [47] overlap drawing of the molecules **4'** and **4''** which constitute the asymmetric unit of **4**.

There is considerable variation in the two molecules that constitute the asymmetric unit of **4** as is evident in an overlap presentation of the two O's and Eu atoms in **4'** and **4''**, Fig. 5. The unit cell did contain eight CH_2Cl_2 molecules and the difference may be a result of sterics resulting from the packing arrangement. One noteworthy difference is in the $\text{N}(1)\text{--Ln}(1)\text{--N}(3)$ angles with $144.66(5)$ and $133.15(6)^\circ$ for **4'** and **4''** respectively, see Table 4. This corresponds to a larger $\text{O}(1)\text{--Ln}(1)\text{--O}(2)$ of $78.33(5)$ for **4''** compared to $72.29(5)^\circ$ for **4'** suggesting that the two ligands, i.e., **2**, have twisted towards the equatorial Cl atom in **4''**. However, the distance between the two H atoms involved in the H-bond to this equatorial Cl ligand is longer in **4''** (4.480 compared to 4.452 Å in **4'**). These effects can be rationalized as the deviation away from pentagonal planarity as evident in the deviations away from 360° in the angles labelled as “equatorial sum” in Table 4. Complex **4''** at 368.7° exhibits the largest deviation but complex **5** at 365.4° is also not planar. This illustrates the flexibility of the coordination sphere around these lanthanide elements.

Currently there are only two structural studies of mononuclear complexes of formulae $\text{TbCl}_3\text{O}_2\text{N}_2$ (none with Sm and Eu) depicting a meridional pentagonal bipyramidal coordination geometry listed in the Cambridge Crystallographic Data Base [50]. The structures consist of O-atom donors from two DMF molecules and N-atom donors in the form of either bidentate dipyrido[3,2-*d*:2',3'-*f*] quinoxaline or dipyrido[3,2-*a*:2',3'-*c*]phenazine ligands binding to the *mer*- TbCl_3 moieties [51]. Two related Sm derivatives were also reported with these ligands but these contained an additional water molecule resulting in a distorted dodecahedral coordination geometry [52]. A mononuclear Eu complex, $\text{EuCl}_3(\text{tptz})(\text{MeOH})_2$, $\text{tptz} = 2,4,6\text{-tris-2-pyridyl-1,3,5-triazine}$ was reported but this also featured a dodecahedral coordination geometry as there were three N-atoms binding from the tptz ligand [53]. These different coordination geometries do not allow for bond angles to be compared in the case of the Sm and Eu complexes and the different ligands used also render meaningless comparisons between the bond angles in **5** and the two Tb complexes [53]. However the bond distances in **5** specifically the Tb–O, Tb–N and Tb–Cl are within the range of distances reported for the two Tb complexes with the *N,N*-bidentate ligands previously reported [53] except for the Tb– $\text{Cl}_{(\text{eq})}$ distance in **5** ($2.7372(5)$ Å) which is significantly longer than the equivalent ones reported (2.678 , 2.673 and 2.670 Å), Table S1. This difference may be due to the fact that this $\text{Cl}_{(\text{eq})}$ ligand is engaged in H-bonding to the H atoms attached to the pyrazole N atoms as shown in Figs. 2–4.

Quantum mechanical calculations on lanthanide compounds are challenging due to the size of the lanthanide ions, and *ab initio* effective core potential calculations have traditionally been used to

make the calculations computationally more manageable. An investigation from 2006 based on 52 lanthanide complexes suggested the RHF/STO-3G/ECP method and basis sets would be most capable of reproducing the coordination polyhedron geometries [54,55]. More sophisticated methods have since been developed, with most based on various Density Functional methods. Challenges [56] and difficulties [57,58] in the DFT method have been noted recently. We decided to test several of the DFT basis sets for conducting theoretical studies on complexes **3–5**, using the Gaussian [33] platform and data from the crystal structures as the starting model. Recently Parker and coworkers used a LanL2DZ (La) basis for calculations on a TbL_3 compound [36] replacing the Tb by La for the purpose of calculations. It is clear given the decrease in bond lengths from complexes **3** to **4** and then **5**, that this would not result in an accurate geometry determination for compounds, and Parker and coworkers restrained the distances between the La and N/O atoms to the values found by X-ray diffraction. The inadequacy of the LanL2DZ (La) basis for use with the other lanthanides without use of distance restraints was confirmed by our calculations. The bond lengths obtained were much longer than those obtained via crystallography for **3** and may indeed be meaningful for the element La, but not for the other lanthanides. We decided to instead use the PBPBE functional with 6-31G* basis sets for the non-lanthanide elements and the Stuttgart RSC 1997 ECP basis set for each individual lanthanide element, i.e., Sm, Eu and Tb. These are available from the Basis Set Exchange [37] Using these specific basis set combinations for **3–5** did result in closer agreement to the X-ray determined data, with a similar decrease in the distances. The results of these calculations are summarized in Table 4, and details for all calculations are given in the SI.

Relationships between the bond distance and angle data from calculated and experimental are not easily drawn. The data from the crystal structures may depict geometric differences purely based on the packing effects of the interstitial solvent molecules and these would be difficult to calculate. Additionally, complex **4** had two molecules in the asymmetric unit and these had significant differences in bond lengths and angles, see Table 4. One could conclude that there was a poor relationship in this case. In particular, the angles in the line labelled as “equatorial sum” in Table 4 are much larger for the calculated structures than those listed for the specific complex, i.e., **3–5**, had more twists in them on average than the X-ray determined structures as the larger related equatorial sum of angles illustrates.

4.3. Luminescent data

The lanthanide complexes absorb at 256 nm for **3**, 257 for **4** and 263 nm for **5** in dichloromethane, a region which corresponds to the $\pi\text{--}\pi^*$ transition in the pyrazole moiety of ligand **2**. Complexes **3–5** display visible fluorescence in the solid and solution states as the image in Fig. S7 attests. The luminescent properties of ligand **2** and complexes **3–5** were assessed in acetonitrile (Figs. S8–S11) and dichloromethane solutions, see Figs. S12 and 6–8. The notable difference between the spectra of complexes **3–5** in these two solvents was the presence of more dissociated ligand **2** in acetonitrile, judging by the increase in the peaks at 309 and 611 nm ascribed to the ligand, Fig. S12. Solutions in acetonitrile lose lanthanide luminescent properties after one day suggesting complete decomposition occurs. Interestingly, ligand **2** absorbs at 249 (253 nm) in acetonitrile (dichloromethane) solutions and emits at 311 (309) and 611 (611) nm. The ligand **2** could be thought of as consisting of the addition of phenylpyrazole (phpz) and methylphenylphosphine oxide. The spectra for these molecules, presented as Fig. S13, reveal that the emission spectra are mostly due to the phenylpyrazole moiety on ligand **2**, judging from the much larger emission spectrum for phpz compared to MePh_2PO . The band at lower

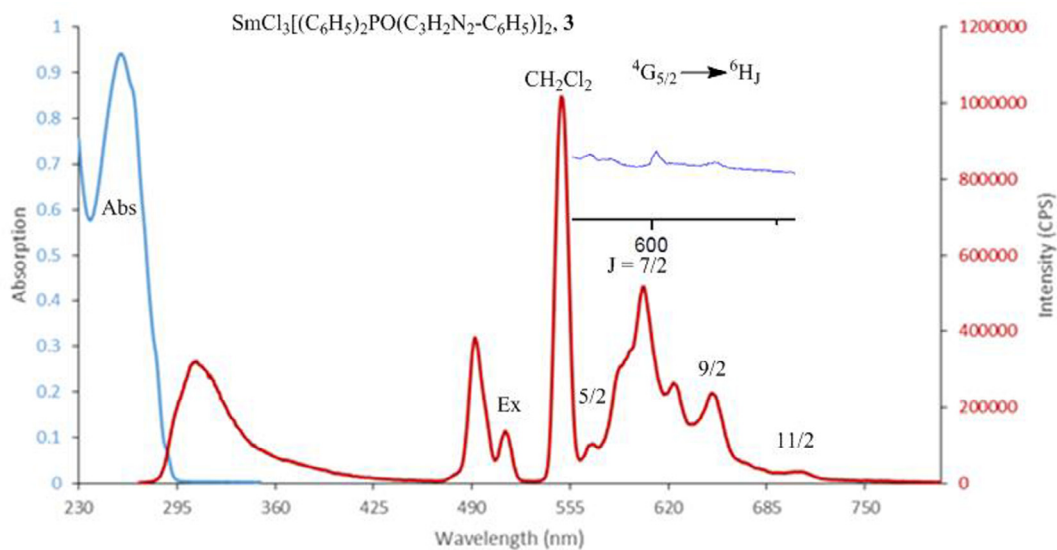


Fig. 6. Absorption (left) and emission (right) spectra for complex **3** dissolved in dichloromethane. The λ_{max} is 258 nm. Inset is the solid state spectrum of **3** in a glass capillary.

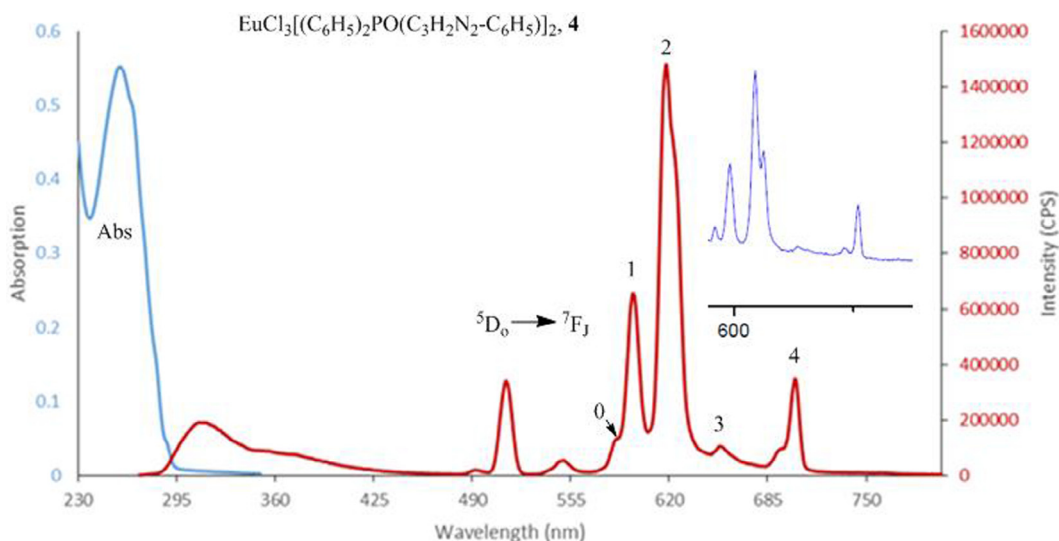


Fig. 7. Absorption (left) and emission (right) spectra for complex **4** dissolved in dichloromethane. The λ_{max} is 257 nm. Inset is the solid state spectrum of **4** in a glass capillary.

energies occurring at roughly twice the wavelength may be assigned as Rayleigh second order scattering [59].

The state symbol designations for the emissions in Figs. 6–8 are based on literature assignments [15,19,22,60,61]. The intensity of the emission spectrum of the samarium based complex **3** is much weaker than that for **4** (Eu) and **5** (Tb), in particular in the solid state, Fig. 6 (see inset). This has been ascribed to a smaller energy difference between the first excited, i.e., $^4G_{5/2}$, and the level immediately below, i.e., $^6H_{11/2}$, which increases the likelihood of nonradiative decay of the excited states [62], which tend to occur at a much faster time scale than radiative transitions. Transitions for complex **3** consists of $^4G_{5/2} \rightarrow ^6H_{11/2}$ (702 nm), $^4G_{5/2} \rightarrow ^6H_{9/2}$ (648 nm), $^4G_{5/2} \rightarrow ^6H_{7/2}$ (603 nm) and $^4G_{5/2} \rightarrow ^6H_{5/2}$ (570 nm) can be identified in the solution spectrum and the last three in the solid state inset spectrum. Large emissions presumably from dissociated ligand at 308 and a bump around 600 nm also appear in the spectrum together with an absorption at 511 nm corresponding to double the excitation wavelength. The transition to $J = 7/2$ is larger than the one to $9/2$. This is presumably because the band between

555 and 685 nm contains the second order spectrum of the ligand emission. Figs. 6–8 also contains what is believed to be Rayleigh scattering from the solvent dichloromethane centered at 548 nm together with a very large anti-Stokes shift at 492 nm and a Stokes absorption overlapping with the large band at 603 nm. The intensity of the solvent scatter is strongest in the spectrum for complex **3**, Fig. 6, much reduced for complex **4**, Fig. 7, and would appear to be overlapping in the spectrum for complex **5**, Fig. 8. In these cases, assignment of the emissions for **4** and **5** can be obtained by examining the solid state profile insets which are free of the solvent contributions.

The spectrum for complex **4** contains transitions $^5D_0 \rightarrow ^7F_4$ (702 nm), $^5D_0 \rightarrow ^7F_3$ (655 nm), $^5D_0 \rightarrow ^7F_2$ (618 nm), $^5D_0 \rightarrow ^7F_1$ (596 nm) and $^5D_0 \rightarrow ^7F_0$ (585 nm) which are all clearly present in the solid state spectrum, Fig. 7. In this case there appears to be less dissociation of the ligand **2** from the complex judging from the reduced intensity of the emission associated with the free ligand. The spectrum for complex **5**, Fig. 8, contains the least dissociated ligand and the following transitions $^5D_4 \rightarrow ^7F_0$ (683 nm), $^5D_4 \rightarrow$

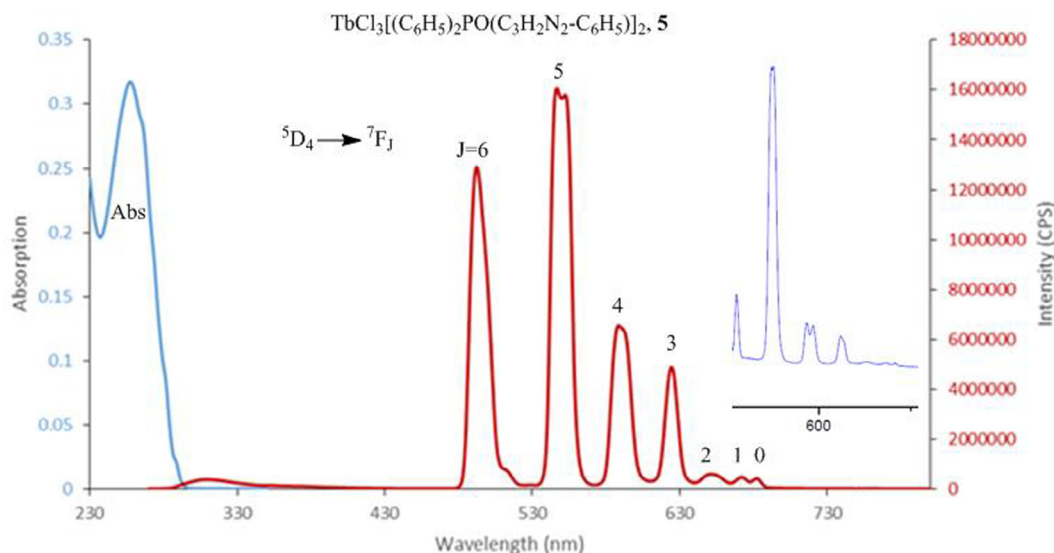


Fig. 8. Absorption and emission spectra for complex **5** dissolved in dichloromethane. The λ_{max} is 257 nm. Inset is the solid state spectrum of **5** in a glass capillary.

7F_1 (672 nm), ${}^5D_4 \rightarrow {}^7F_2$ (650 nm), ${}^5D_4 \rightarrow {}^7F_3$ (626 nm), ${}^5D_4 \rightarrow {}^7F_4$ (590 nm), ${}^5D_4 \rightarrow {}^7F_5$ (552 nm) and ${}^5D_4 \rightarrow {}^7F_6$ (494 nm) in solution. These emissions are also observed in the solid state with fine structure discernible in some cases, see inset Fig. 8.

The efficiency of the transduction of light from the ligand to the lanthanide element was assessed using a comparative method [30] with tyrosine which has a known Φ_F of 0.14 [63]. Due to the instability of the complexes in solution as noted above, this measurement was only obtained for complex **5** in dichloromethane. The quantum yield of ligand **2** was found to be similar to that of tyrosine at 0.15 but that for complex **5** was assessed close to 1.00. It is believed that this method has a large error of up to 20% [64]. However, the fact remains that the energy transfer was qualitatively very efficient. Interestingly, the graphs in Figs. 6–8 do show that the intensity of the emission spectra increased from complex **3** to **5**. One reason for this could be better energy transfer in complex **5**. Interestingly the distances between the lanthanide element and the O- and N-atoms that bind from **2** to the lanthanide element also decrease from complex **3** to **5**, see Table 4. This shorter distance in complex **5** may result in a greater stability in solution (in acetonitrile) and may also be the reason for the highest intensity in the emission spectrum compared to complexes **3** and **4**.

5. Conclusions

The bidentate ligand, diphenyl((5-phenyl-4H-1 λ^4 -pyrazol-3-yl)methyl)phosphine oxide, **2**, was synthesized and shown to undergo proton transfer between the N-atoms on the pyrazolyl moiety. Variable temperature NMR measurements estimated an activation barrier for this process of ca. 14.4–14.9 kcal/mol in close agreement with calculated values of 13.63 and 14.08 kcal/mol for a mechanism involving two water molecules. Three lanthanide complexes of formulae $\text{LnCl}_3(\mathbf{2})_2$, Ln = Sm, Eu and Tb, were prepared and verified to have pentagonal bipyramidal geometries by single-crystal X-ray diffraction. The bidentate ligands were located in the pseudo-equatorial plane with the chloride ligands in a meridional conformation. The thermal decomposition of these complexes as verified by TGA measurements was not cleanly defined, but appeared to consist of the slow decomposition of the two ligands leaving behind mostly the trihalide species. The complexes were not stable in acetonitrile solutions for long periods and their emissive properties were assessed in both acetonitrile and

dichloromethane solutions. The photoluminescent properties of the complexes were illustrated in both solid and solution forms and the emission spectra were found to be identical to relaxation pathways previously assigned to the specific lanthanide ion. This report demonstrates the feasibility of ligand **2** as a sensitizing agent for emissions with metal ions with the terbium complex, **5**, having a very high quantum efficiency for the transfer.

Acknowledgements

The diffractometer used to solve the structures was funded by NSF Grant 0087210, by Ohio Board of Regents Grant CAP-491, and by Youngstown State University. Support by Michigan Technological University is acknowledged. Helpful comments by the reviewers, in particular, comments on the emission spectra, are gratefully acknowledged.

Appendix A. Supplementary data

CCDC's 1528931–1528933 contain the supplementary crystallographic data for complexes **3–5** respectively. These data can be obtained free of charge from The Cambridge Crystallographic Data Center via www.ccdc.cam.ac.uk/data_request/cif. Supplementary data associated with this article can be found, in the online version, at <https://doi.org/10.1016/j.ica.2017.11.049>.

References

- [1] L. Feng, J.S. Maass, R.L. Luck, Synthesis and characterization of four cubical molybdenum(V) tetramers and their catalytic properties for the epoxidation of cis-cyclooctene using H_2O_2 , *Inorg. Chim. Acta* 373 (1) (2011) 85–92.
- [2] L. Feng, E. Urnezis, R.L. Luck, Cyclooctene epoxidation with H_2O_2 and single crystal X-ray determined crystal structures of new molybdenum and tungsten catalysts bearing the hydrophilic ligand hydroxymethyldiphenylphosphine oxide, *J. Organomet. Chem.* 693 (8–9) (2008) 1564–1571.
- [3] A. Jimtaisong, R.L. Luck, In Epoxidation of Cis-Cyclooctene Using Hydrogen Peroxide in Ethanol with Catalysts $\text{MCl}_2\text{O}_2(\text{OPR}_3)_2$ (M = Mo, W and $\text{OPR}_3 = (\text{OPMePh}_2)$, $1/2\text{dppmO}_2$) and $\text{WO}(\text{O}_2)_2(\text{dppmO}_2)$: Catalytic Reactivities and Crystal Structures of $\text{WCl}_2\text{O}_2(\text{dppmO}_2)$ and $\text{WO}(\text{O}_2)_2(\text{dppmO}_2)$ will be Featured, American Chemical Society, 2006. pp. INOR-544.
- [4] A. Jimtaisong, R.L. Luck, Synthesis and catalytic epoxidation activity with TBHP and H_2O_2 of dioxo-, oxoperoxo-, and oxodiperoxo molybdenum(VI) and tungsten(VI) compounds containing monodentate or bidentate phosphine oxide ligands: crystal structures of $\text{WCl}_2(\text{O})_2(\text{OPMePh}_2)_2$, $\text{WCl}_2(\text{O})(\text{O}_2)(\text{OPMePh}_2)_2$, $\text{MoCl}_2(\text{O})_2\text{dppmO}_2\text{C}_4\text{H}_{10}$, $\text{WCl}_2(\text{O})_2\text{dppmO}_2$, $\text{Mo}(\text{O})(\text{O}_2)_2\text{dppmO}_2$, and $\text{W}(\text{O})(\text{O}_2)_2\text{dppmO}_2$, *Inorg. Chem.* 45 (25) (2006) 10391–10402.

- [5] J.S. Maass, M. Zeller, T.M. Breault, B.M. Bartlett, H. Sakiyama, R.L. Luck, Syntheses and structures of three complexes of formulas $[L_3Co(\mu_2-O_2P(Bn)_2)_3Co]^{2+}$, featuring octahedral and tetrahedral cobalt(II) geometries; variable-temperature magnetic susceptibility measurement and analysis on $[(py)_3Co(\mu_2-O_2P(Bn)_2)_3Co(py)]^{2+}$, *Inorg. Chem.* 51 (9) (2012) 4903–4905.
- [6] J.S. Maass, Z. Chen, M. Zeller, R.L. Luck, Syntheses and characterization of the vanadium trimer $(V_3(\mu_3-O)_2)(\mu_2-O_2P(CH_2C_6H_5)_2)_6(4,4'-bipyridine)$ and the vanadium hexamer $[(V_3(\mu_3-O)_2)(\mu_2-O_2P(CH_2C_6H_5)_2)_6]_2(\mu_2-N_1, N_2-di(pyridin-4-yl)oxalamide)$, *J. Coord. Chem.* 69 (15) (2016) 2342–2352.
- [7] J.S. Maass, M. Zeller, R.L. Luck, Synthesis and crystal structure of the octametallic ferrocene containing molybdenum(V) cluster $Mo_4(\mu_3-O)_4(\mu_2-O_2P(CH_2)_2Fc)_4O_4$ and crystal structure of 1,1'-bis(Chloromethyl)ferrocene, *J. Cluster Sci.* 23 (3) (2012) 713–726.
- [8] J.S. Maass, Z. Chen, M. Zeller, F. Tuna, R.E.P. Winpenny, R.L. Luck, Syntheses, X-ray structural characterizations, and thermal stabilities of two nonclassical trinuclear vanadium(IV) complexes, $(V_3(\mu_3-O)_2)(\mu_2-O_2P(CH_2C_6H_5)_2)_6(H_2O)$ and $(V_3(\mu_3-O)_2)(\mu_2-O_2P(CH_2C_6H_5)_2)_6(py)$, and polymeric complexes of stoichiometry $(VO(O_2PR)_2)_\infty$, $R^2 = Ph$ and $o-(CH_2)_2(C_6H_4)$, *Inorg. Chem.* 51 (5) (2012) 2766–2776.
- [9] J.S. Maass, M. Zeller, D. Holmes, C.A. Bayse, R.L. Luck, Syntheses, ^{95}Mo NMR spectroscopy and structures of distorted cubic $Mo_4(\mu_3-O)_4(\mu_2-O_2P(CH_2C_6H_5)_2)_4O_4$ and the open mixed-valent cluster, $Mo_4(\mu_3-O)_2(\mu_2-O_2P(CH_2C_6H_5)_2)_6O_6$, *J. Cluster Sci.* 22 (2) (2011) 193–210.
- [10] J.S. Maass, Z. Chen, M. Zeller, R.L. Luck, Expanding molecular transition metal cubane clusters of the form $[M_4(\mu_3-O)_4]_{12+}$: syntheses, spectroscopic and structural characterizations of molecules $M_4(\mu_3-O)_4(O_2P(Bn)_2)_4(O_4)$, $M = V$ and W , *Dalton Trans.* 40 (43) (2011) 11356–11358.
- [11] S. Mal, M. Pietraszkiwicz, O. Pietraszkiwicz, Strongly photoluminescent Eu(III) tetrazolate ternary complexes with phosphine oxides as powerful sensitizers, *J. Coord. Chem.* 68 (2) (2015) 367–377.
- [12] S. Mal, M. Pietraszkiwicz, O. Pietraszkiwicz, Synthesis and photophysical studies of tetrazolate-based Eu(III) photoluminescent ternary complexes containing N-heterocyclic phosphine oxides auxiliary co-ligands, *Luminescence* 31 (5) (2016) 1085–1090.
- [13] X.-K. Liu, C.-J. Zheng, M.-F. Lo, J. Xiao, C.-S. Lee, M.-K. Fung, X.-H. Zhang, A multifunctional phosphine oxide-diphenylamine hybrid compound as a high performance deep-blue fluorescent emitter and green phosphorescent host, *Chem. Commun.* 50 (16) (2014) 2027–2029.
- [14] H. Xu, L.-H. Wang, X.-H. Zhu, K. Yin, G.-Y. Zhong, X.-Y. Hou, W. Huang, Application of chelate phosphine oxide ligand in Eu(III) complex with mezzo triplet energy level, highly efficient photoluminescent, and electroluminescent performances, *J. Phys. Chem. B* 110 (7) (2006) 3023–3029.
- [15] Y. Hirai, T. Nakanishi, Y. Hasegawa, Organo-lanthanide luminescences bridged by phosphine oxide ligands, *J. Lumin.* 170 (2016) 801–807.
- [16] A. Mangalum, R.C. Smith, Bifunctional cross-conjugated luminescent phosphines and phosphine derivatives: phospho-cruciforms, *Dalton Trans.* 39 (21) (2010) 5145–5151.
- [17] R.G. Pearson, Hard and soft acids and bases, *J. Am. Chem. Soc.* 85 (22) (1963) 3533–3539.
- [18] A. de Bettencourt-Dias, J.S.K. Rossini, Ligand design for luminescent lanthanide-containing metallopolymer, *Inorg. Chem.* 55 (20) (2016) 9954–9963.
- [19] Y. Hasegawa, S.-I. Tsuruoka, T. Yoshida, H. Kawai, T. Kawai, Enhanced deep-red luminescence of tris(hexafluoroacetylacetonato)samarium(III) complex with phenanthroline in solution by control of ligand coordination, *J. Phys. Chem. A* 112 (5) (2008) 803–807.
- [20] T. Fei, X. Gu, M. Zhang, C. Wang, M. Hanif, H. Zhang, Y. Ma, Optical and electronic properties of phosphorescent iridium(III) complexes with phenylpyrazole and ancillary ligands, *Synth. Met.* 159 (1) (2009) 113–118.
- [21] Z. Ahmed, K. Iftikhar, Efficient photoluminescent complexes of 400–1800 nm wavelength emitting lanthanides containing organic sensitizers for optoelectronic devices, *RSC Adv.* 4 (109) (2014) 63696–63711.
- [22] A. Aebischer, F. Gummy, J.-C.G. Bunzli, Intrinsic quantum yields and radiative lifetimes of lanthanide tris(dipicolinate)s, *PCCP* 11 (9) (2009) 1346–1353.
- [23] D. Parker, J.W. Walton, L. Lamarque, J.M. Zwier, Comparative study of the luminescence properties and relative stability of a series of europium(III) complexes bearing one to four coordinated azaxanthone groups, *Eur. J. Inorg. Chem.* 2010 (25) (2010) 3961–3966.
- [24] Deni, J. Nordmann, J. Dziambor, B. Mayer, W. Frank, T.J.J. Muller, Sequential palladium catalyzed coupling-cyclocondensation-coupling (C3) four-component synthesis of intensively blue luminescent biarylsubstituted pyrazoles, *RSC Adv.* 5 (43) (2015) 33838–33854.
- [25] D.S. Bolotin, M.V. Il'in, I.E. Kolesnikov, V.V. Suslonov, Y. Novozhilov, O. Ronzhina, M. Krasavin, V.P. Boyarskiy, R. Koen, A. Roodt, Fluorescent (pyrazolyl acetoxime)ZnII complexes: synthetic, structural, and photophysical studies, *Inorg. Chim. Acta* 455 (Part 1) (2017) 9–14.
- [26] K. Binemans, Lanthanide-based luminescent hybrid materials, *Chem. Rev.* 109 (9) (2009) 4283–4374.
- [27] M. Sy, A. Nonat, N. Hildebrandt, L.J. Charbonniere, Lanthanide-based luminescence biolabelling, *Chem. Commun.* 52 (29) (2016) 5080–5095.
- [28] Y. Liu, D. Tu, H. Zhu, X. Chen, Lanthanide-doped luminescent nanoprobe: controlled synthesis, optical spectroscopy, and bioapplications, *Chem. Soc. Rev.* 42 (16) (2013) 6924–6958.
- [29] D. Geißler, S. Linden, K. Liermann, K.D. Wegner, L.J. Charbonniere, N. Hildebrandt, Lanthanides and quantum dots as Förster resonance energy transfer agents for diagnostics and cellular imaging, *Inorg. Chem.* 53 (4) (2014) 1824–1838.
- [30] A.T.R. Williams, S.A. Winfield, J.N. Miller, Relative fluorescence quantum yields using a computer-controlled luminescence spectrometer, *Analyst* 108 (1290) (1983) 1067–1071.
- [31] Bruker Apex2 v2.1-4, Bruker AXS Inc., Madison (WI), USA, 2007.
- [32] G.M. Sheldrick, T.R. Schneider, W. Charles, R.M.S. Carter Jr., [16] SHELXL: high-resolution refinement, in: *Methods Enzymol.*, vol. 277, Academic Press, 1997, pp. 319–343.
- [33] M.J. Frisch, G.W. Trucks, H.B. Schlegel, G.E. Scuseria, M.A. Robb, J.R. Cheeseman, G. Scalmani, V. Barone, B. Mennucci, G.A. Petersson, H. Nakatsuji, M. Caricato, X. Li, H.P. Hratchian, A.F. Izmaylov, J. Bloino, G. Zheng, J.L. Sonnenberg, M. Hada, M. Ehara, K. Toyota, R. Fukuda, J. Hasegawa, M. Ishida, T. Nakajima, Y. Honda, O. Kitao, H. Nakai, T. Vreven, J.A. Montgomery, J.E. Peralta, F. Ogliaro, M. Bearpark, J.J. Heyd, E. Brothers, K.N. Kudin, V.N. Staroverov, R. Kobayashi, J. Normand, K. Raghavachari, A. Rendell, J.C. Burant, S.S. Iyengar, J. Tomasi, M. Cossi, N. Rega, J.M. Millam, M. Klene, J.E. Knox, J.B. Cross, V. Bakken, C. Adamo, J. Jaramillo, R. Gomperts, R.E. Stratmann, O. Yazyev, A.J. Austin, R. Cammi, C. Pomelli, J.W. Ochterski, R.L. Martin, K. Morokuma, V.G. Zakrzewski, G.A. Voth, P. Salvador, J.J. Dannenberg, S. Dapprich, A.D. Daniels, J.B. Farkas, J. Foresman, J.V. Ortiz, J. Cioslowski, D.J. Fox, Gaussian 09, Revision D.01, Wallingford CT, 2013.
- [34] A.D. Becke, Density-functional thermochemistry. III. The role of exact exchange, *J. Chem. Phys.* 98 (7) (1993) 5648–5652.
- [35] C. Lee, W. Yang, R.G. Parr, Development of the Colle-Salvetti correlation-energy formula into a functional of the electron density, *Phys. Rev. B* 37 (2) (1988) 785–789.
- [36] J.W. Walton, L.D. Bari, D. Parker, G. Pescitelli, H. Puschmann, D.S. Yufit, Structure, resolution and chiroptical analysis of stable lanthanide complexes of a pyridylphenylphosphinate triazacyclononane ligand, *Chem. Commun.* 47 (45) (2011) 12289–12291.
- [37] K.L. Schuchardt, B.T. Didier, T. Elsethagen, L. Sun, V. Gurmooorthi, J. Chase, J. Li, T.L. Windus, Basis set exchange: a community database for computational sciences, *J. Chem. Inf. Model.* 47 (3) (2007) 1045–1052.
- [38] M.D. Hanwell, D.E. Curtis, D.C. Lonie, T. Vandermeersch, E. Zurek, G.R. Hutchison, Avogadro: an advanced semantic chemical editor, visualization, and analysis platform, *J. Cheminf.* 4 (1) (2012) 17.
- [39] N.M. O'Boyle, A.L. Tenderholt, K.M. Langner, Cclib: a library for package-independent computational chemistry algorithms, *J. Comput. Chem.* 839–845 (2008).
- [40] R.H. Wiley (Ed.), *Chemistry of Heterocyclic Compounds, Vol. XXII: Pyrazoles, Pyrazolines, Pyrazolidines, Indazoles, and Condensed Rings*, Interscience, 1967, p. 10.
- [41] X. Chen, J. She, Z.-C. Shang, J. Wu, P. Zhang, Room-temperature synthesis of pyrazoles, diazepines, β -enaminones, and β -enamino esters using silica-supported sulfuric acid as a reusable catalyst under solvent-free conditions, *Synth. Commun.* 39 (6) (2009) 947–957.
- [42] J. Sandström, *Dynamic NMR Spectroscopy*, Academic Press, 1982.
- [43] K.D. Zimmer, R. Shoemaker, R.R. Ruminiski, Synthesis and characterization of a fluxional Re(I) carbonyl complex $fac-[Re(CO)_3(dppof')Cl]$ with the nominally tri-dentate ligand $dipyrido(2,3-a:3',2'-j)phenazine$ ($dppof'$), *Inorg. Chim. Acta* 359 (5) (2006) 1478–1484.
- [44] I. Alkorta, J. Elguero, 1,2-Proton shifts in pyrazole and related systems: a computational study of [1,5]-sigmatropic migrations of hydrogen and related phenomena [dagger], *J. Chem. Soc., Perkin Trans. 2* (11) (1998) 2497–2504.
- [45] S. Schweiger, G. Rauhut, Double proton transfer reactions with plateau-like transition state regions: pyrazole–trifluoroacetic acid clusters, *J. Phys. Chem. A* 110 (8) (2006) 2816–2820.
- [46] J.L. Brown, B.L. Davis, B.L. Scott, A.J. Gaunt, Early-lanthanide(III) acetonitrile-solvento adducts with iodide and noncoordinating anions, *Inorg. Chem.* 54 (24) (2015) 11958–11968.
- [47] C.F. Macrae, I.J. Bruno, J.A. Chisholm, P.R. Edgington, P. McCabe, E. Pidcock, L. Rodriguez-Monge, R. Taylor, J. van de Streek, P.A. Wood, Mercury CSD, 2.0 – new features for the visualization and investigation of crystal structures, *J. Appl. Crystallogr.* 41 (2008) 466–470.
- [48] G. Sheldrick, A short history of SHELX, *Acta Crystallogr. A* 64 (1) (2008) 112–122.
- [49] P. D'Angelo, A. Zitolo, V. Migliorati, G. Chillemi, M. Duval, P. Vitorge, S. Abadie, R. Spezia, Revised ionic radii of lanthanoid(III) ions in aqueous solution, *Inorg. Chem.* 50 (10) (2011) 4572–4579.
- [50] F.H. Allen, The Cambridge structural database: a quarter of a million crystal structures and rising, *Acta Crystallogr. B* 58 (2002) 380–388.
- [51] S. Dasari, A.K. Patra, Trichloro-bis(*N,N*-dimethylformamide)-(pyrazino[2,3-*f*][1,10]phenanthroline)-terbium unknown solvate, *Dalton Trans.* 44 (2015) 19844.
- [52] S. Dasari, Z. Abbas, P. Kumar, A.K. Patra, Aqua-trichloro-bis(*N,N*-dimethylformamide)-(pyrazino[2,3-*f*][1,10]phenanthroline)-samarium, *CrystEngComm* 18 (2016) 4313.
- [53] R. Wietzke, M. Mazzanti, J.-M. Latour, J. Pecaut, Bis(methanol)-(2,4,6-tris(2-pyridyl)-1,3,5-triazine)-trichloro-europium(III) methanol solvate, *Inorg. Chem.* 38 (1999) 3581.
- [54] R.O. Freire, N.B. da Costa, G.B. Rocha, A.M. Simas, Sparkle/AM1 parameters for the modeling of samarium(III) and promethium(III) complexes, *J. Chem. Theory Comput.* 2 (1) (2006) 64–74.
- [55] R.O. Freire, G.B. Rocha, A.M. Simas, Lanthanide complex coordination polyhedron geometry prediction accuracies of ab initio effective core potential calculations, *J. Mol. Model.* 12 (4) (2006) 373–389.
- [56] A.J. Cohen, P. Mori-Sánchez, W. Yang, Challenges for density functional theory, *Chem. Rev.* 112 (1) (2012) 289–320.

- [57] S. Hammes-Schiffer, A conundrum for density functional theory, *Science* 355 (6320) (2017) 28–29.
- [58] M.G. Medvedev, I.S. Bushmarinov, J. Sun, J.P. Perdew, K.A. Lyssenko, Density functional theory is straying from the path toward the exact functional, *Science* 355 (6320) (2017) 49–52.
- [59] J.F. Liu, N.B. Li, H.Q. Luo, Resonance Rayleigh scattering, second-order scattering and frequency doubling scattering spectra for studying the interaction of erythrosine with Fe(phen)₃²⁺ and its analytical application, *Spectrochim. Acta Part A Mol. Biomol. Spectrosc.* 79 (3) (2011) 631–637.
- [60] S.V. Eliseeva, M. Ryazanov, F. Gumy, S.I. Troyanov, L.S. Lepnev, J.-C.G. Bünzli, N. P. Kuzmina, Dimeric complexes of lanthanide(III) hexafluoroacetylacetonates with 4-cyanopyridine N-oxide: synthesis, crystal structure, magnetic and photoluminescent properties, *Eur. J. Inorg. Chem.* 2006 (23) (2006) 4809–4820.
- [61] C. Sun, P. Zhao, M. Wei, Z. Chang, W. Li, Synthesis, structure, and fluorescent properties of lanthanide complexes based on 8-hydroxyquinoline-7-carboxylic acid, *Z. Anorg. Allg. Chem.* 642 (5) (2016) 372–376.
- [62] A.N. Gusev, V.F. Shul'gin, S.B. Meshkova, M. Hasegawa, G.G. Alexandrov, I.L. Eremenko, W. Linert, Structural and photophysical studies on ternary Sm(III), Nd(III), Yb(III), Er(III) complexes containing pyridyltriazole ligands, *Polyhedron* 47 (1) (2012) 37–45.
- [63] R.F. Chen, Fluorescence quantum yields of tryptophan and tyrosine, *Anal. Lett.* 1 (1) (1967) 35–42.
- [64] J.B. Birks, Fluorescence quantum yield measurements, *J. Res. Natl. Bur. Stand. Sect. A* 80A (3) (1976) 389–399.